EPJ Web of Conferences **182**, 02067 (2018) https://doi.org/10.1051/epjconf/201818202067
ICNFP 2017

Measurements of the Vector boson production with the ATLAS Detector

Kostas KORDAS[1,a] , On behalf of the ATLAS Collaboration

[1] *Department of Physics, Aristotle University of Thessaloniki, Thessaloniki, GR-54124 Greece*

Abstract. The electroweak sector of the Standard Model can be tested by precision measurements of its fundamental parameters, such as the W boson mass or the electroweak mixing angle. In this contribution we present the first measurement of the W boson mass, based on the 7 TeV data set corresponding to an integrated luminosity of 4.6 fb^{-1}. With this data set the detector and physics modelling have been studied in great detail, leading to an overall uncertainty of 19 MeV. The ATLAS collaboration also performed a new precise triple differential Z/γ^* Drell-Yan cross-section measurement as a function of the dilepton mass, the dilepton rapidity and $\cos\theta^*$ defined in the Collins-Soper frame. This measurement provides sensitivity to the PDFs and the Z forward-backward asymmetry, A_{FB}, which is derived and will be presented. The latter builds the foundation for a possible future extraction of the weak-mixing angle. The production of jets in association with vector bosons is an important process to study perturbative QCD in a multi-scale environment. The ATLAS collaboration has performed new measurements of vector boson plus jets cross sections, differential in several kinematic variables, in proton-proton collision data, taken at center-of-mass energies of 8 TeV and 13 TeV. These measurements are presented and compared to state-of-the art theory predictions. They are sensitive to higher-order pQCD effects, and can be used to constrain the proton structure. In addition, we present a new measurement of the splitting scales of the k_{t} jet-clustering algorithm for final states containing a Z-boson candidate at a centre-of-mass energy of 8 TeV.

1 Introduction

The electroweak sector of the Standard Model (SM) can be tested by precision measurements of fundamental parameters, such as the W boson mass (m_W) and the electroweak mixing angle ($\sin^2\theta_W$). In addition, precise cross section measurements of W and Z production constrain the Parton Distribution Functions (PDFs) and are sensitive probes of higher order QCD corrections. In this note a collection of various ATLAS [1] measurements on these topics are presented, starting with the measurement of the W mass [2] which is determined with an overall uncertainty of 19 MeV, on par with the best single measurement to-date from CDF [3]. Then, inclusive production measurements of W and Z bosons are presented, where unprecedented precision and strong constraints on PDFs, in particular the strange-quark density, are obtained [4]. The production of Z bosons in various jet multiplicities is presented next [5], as well as a measurement of the jet splitting scales in such events [6]; these measurements

[a] e-mail: kordas@physics.auth.gr

are compared to state-of-the art theory predictions. Last, the triple differential cross section of the Z/γ^* Drell-Yan production is presented [7] and the forward-backward asymmetry is derived, which forms the base for a future measurement of the electroweak mixing angle.

2 W mass measurement

At lowest order in the electroweak theory, the W-boson mass, m_W, can be expressed solely as a function of the Z-boson mass, m_Z , the fine-structure constant, α, and the Fermi constant, G_F . Higher-order corrections introduce an additional dependence on the gauge couplings and the masses of the heavy particles of the SM. Thus, in the SM the W-boson mass is particularly sensitive to the top-quark and Higgs-boson masses, while in theories beyond the SM the W mass receives contributions from additional particles and interactions. These effects can be probed by comparing the measured and predicted values of m_W . The world average value is $m_W = 80385 \pm 15$ MeV [8], driven by the CDF measurement [3]. Given the precisely measured values of α, G_F and m_Z , and recent top and Higgs mass measurements [8], the SM prediction is $m_W = 80356 \pm 8$ MeV according to Ref. [9] and $m_W = 80362 \pm 8$ MeV according to Ref. [10]. In the context of global fits to the SM parameters, constraints on physics beyond the SM are currently limited by the W-boson mass measurement precision [9]; thus, 8 MeV is a good target for the precision of the measured W mass.

Data collected by ATLAS at $\sqrt{s} = 7$ TeV pp collisions are used for the measurement reported here [2]. The W mass is measured in decays of the W to leptons, $W^- \to \ell^- \bar{\nu}_\ell$ and their charge conjugate decays, with ℓ denoting electrons or muons. In such events the W mass is derived from fits to the distributions of the lepton p_{T} ($p_{\mathrm{T}}{}^{\ell}$) and the W-boson m_{T}, where $m_{\mathrm{T}} = \sqrt{2\, p_{\mathrm{T}}^{\ell}\, p_{\mathrm{T}}^{\mathrm{miss}}\, (1 - \cos\Delta\phi)}$ is the transverse mass of the W boson; $\vec{p}_{\mathrm{T}}^{\,\mathrm{miss}} = -(\vec{p}_{\mathrm{T}}^{\,\ell} + \vec{u}_{\mathrm{T}})$ is the missing transverse momentum; $\vec{u}_{\mathrm{T}}$ is the transverse momentum of the "recoil" accompanying the produced W, determined from the vector sum of all energy deposits in the calorimeter excluding the one from the lepton; and $\Delta\phi$ is the azimuthal opening angle between the charged lepton and the missing transverse momentum.

Template distributions for various m_W values are compared to the observed $p_{\mathrm{T}}{}^{\ell}$ and m_{T} distributions, and this yields m_W based on a χ^2 test. The templates are affected by the modeling of both the background and the signal, with the later dominating by far the uncertainty of the measurement. The effects on the signal modelling are classified in two broad categories: the "physics modelling" (the description of the W recoil, the p_{T} distribution of the W, the fraction of W-bosons produced in the various helicity states, and the proton PDFs), and the "detector response" (energy and momentum calibration, as well as lepton identification and reconstruction efficiencies). $Z \to e^+e^-$ and $Z \to \mu^+\mu^-$ events are used to calibrate the detector, control the physics modelling and validate the mass extraction method. The mass of the W-boson is extracted in various categories (electron/muon decay channels, lepton charge and pseudorapidity), with both the $p_{\mathrm{T}}{}^{\ell}$ and m_{T} methods, for cross-checking. The final W mass is obtained from the combination of all these measurements. An overview of the various m_W determinations and their weights in the overall combination is shown is Figure 1.

The systematics from the physics modelling amount to 14 MeV. The largest contribution comes from the PDFs, which improves in the combination of W^+ and W^- to become 9.2 MeV. The next two biggest contributions, at $\simeq 6$ MeV each, are from the uncertainty on the W p_{T} and from the angular coefficients in the description of the fraction of the W bosons produced in the different polarization states. Both of these sources of uncertainty have a similar effect on m_W between the W^+ and W^- states and between the $p_{\mathrm{T}}{}^{\ell}$ and m_T kinematics. The QED / ElectroWeak modelling of the final state radiation, and the interference between the initial and final state radiations contribute 5.5 MeV to the m_W uncertainty.

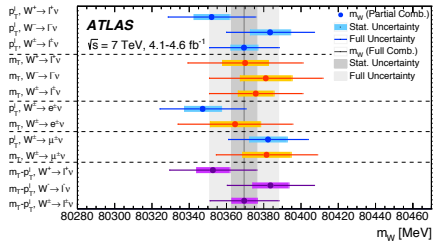

Combination	Weight
Electrons	0.427
Muons	0.573
m_{T}	0.144
p_{T}^{ℓ}	0.856
W^+	0.519
W^-	0.481

Figure 1: *Left:* Overview of the m_W determinations from the ${p_{\mathrm{T}}}^{\ell}$ and m_{T} distributions, and for the combination of the ${p_{\mathrm{T}}}^{\ell}$ and m_{T} distributions, in the muon and electron decay channels and for W^+ and W^- events. The horizontal lines and bands show the statistical and total uncertainties of the individual m_W determinations. The combined result for m_W, its statistical and total uncertainties are also indicated (vertical line and bands). *Right:* Total weights of the electron and muon channels, of the m_{T} and ${p_{\mathrm{T}}}^{\ell}$ distributions, and of the W^+ and W^- samples in the overall combination to extract m_W, for the optimal fitting range ($32 < p_{\mathrm{T}}^{\ell} < 45$ GeV, $66 < m_{\mathrm{T}} < 99$ GeV) used for the fit [2].

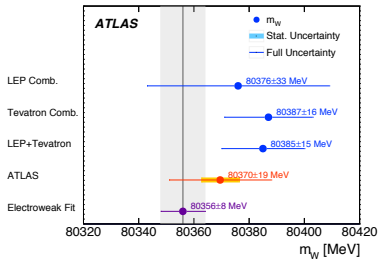

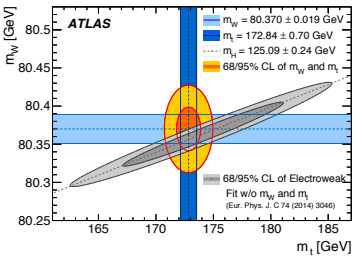

Figure 2: *Left:* The measured value of m_W is compared to other published results. The vertical band shows the uncertainty of the theoretical prediction [9], and the horizontal bands and lines show the statistical and total uncertainties of the ATLAS and other published results. *Right:* The 68% and 95% confidence-level contours of the W and top masses determined indirectly from the global electroweak fit [9], are compared to the respective ATLAS measurements, shown with the equivalent confidence-level contours [2].

The systematics from experimental sources amount to 11 MeV, dominated by the lepton uncertainties. Momentum scale and resolution corrections are derived from $Z \to \ell^+\ell^-$ data, and are extrapolated to the W boson using the lepton p_{T} spectra. "Sagitta biases" (from detector displacements and twists) are studied from Z events again and from E/p measurements in $W \to e\nu$ decays. The electron and muon uncertainties contribute 6.4 MeV and 6.6 MeV, respectively, to the m_W determination. The response of the detector to the recoil and the modelling of the background contribute 2.9 MeV and 4.5 MeV, respectively.

With a 7 MeV statistical uncertainty on the combined m_W measurement, ATLAS achieves an overall uncertainty of 19 MeV, equal to that of the single best measurement to date from CDF [3], and reports [2]: $m_W = 80370 \pm 19$ MeV. In Figure 2 this measurement is compared to other published results and to the indirect determination from the global electroweak fit. The ATLAS measurement brings the measured world average closer to the electroweak fit.

3 W and $Z/\gamma^\star$ production cross sections

Measurements of the Drell-Yan production of W and $Z/\gamma^\star$ bosons at the LHC provide a benchmark of our understanding of perturbative QCD and probe the proton structure in a unique way.

Here, recent high-precision measurements by the ATLAS Collaboration are presented for the inclusive $W^+ \to \ell^+\nu$, $W^- \to \ell^-\bar{\nu}$ and $Z/\gamma^\star \to \ell^+\ell^-$ Drell-Yan production at the LHC (with ℓ denoting as before electrons and muons) [4], using data of an integrated luminosity of 4.6 fb^{-1} collected in proton–proton collisions at $\sqrt{s} = 7$ TeV. Differential W^+ and W^- cross sections are measured in a lepton pseudorapidity range $|\eta| < 2.5$. Differential $Z/\gamma^\star$ cross sections are measured as a function of the absolute dilepton rapidity, for $|y| < 3.6$, for three intervals of dilepton mass, m , extending from 46 to 150 GeV. The results report "fiducial" cross sections, corresponding to the reduced phase-space of the measurements, including the branching ratios for the decay channels.

Integrated measurements for W and Z production cross section in the electron and muon decay channels are also derived. These measurements, extrapolated to a common fiducial phase space, are used to form cross section ratios, where luminosity uncertainties cancel. Ratios between the electron and muon channels of the same boson are sensitive to lepton universality. From the ratio of the W electronic and muonic cross sections (for each channel the W boson cross section is the sum of the W$^+$ and W$^-$ cross sections) the ratio $R_W = BR(W \to e\nu)/BR(W \to \mu\nu)$ is obtained. The ATLAS result of $R_W = 0.997 \pm 0.010$ is more precise than the combination of LEP results from $e^+e^- \to W^+W^-$ data, as well as from the CDF and LHCb results (see Ref. [4] and references therein). The corresponding ratio of Z boson cross sections yields $R_Z = BR(Z \to e^+e^-)/BR(Z \to \mu^+\mu^-) = 1.0026 \pm 0.0050$, which agrees well with the value obtained from the combination of $e^+e^- \to Z$ data from LEP and SLC of 0.9991 ± 0.0028 [11]. The ratio of W^+ to W^- and of the $W^\pm$ sum to the Z cross sections is sensitive to the PDFs, as seen in Figure 3. The predictions for the ratio $W^\pm/Z$ are systematically higher than in the data, and this is investigated further with the differential cross sections as a function of rapidity.

The lepton charge asymmetry, A_ℓ, in W decays, defined as the difference between the W^+ and W^- cross sections over their sum, is shown as a function of the lepton pseudorapidity in Figure 4, left. The data have an accuracy of better than 1% and it is seen that in general all PDFs agree with the data. The best description is given by NNPDF3.0 which uses W charge asymmetry data from CMS [12], but, as shown in Ref. [4], it does not describe well the separate pseudorapidity distributions of ℓ^+ and ℓ^-. The HERAPDF2.0 PDF follows well both the charge asymmetry as seen in Figure 4, and the individual ℓ^+

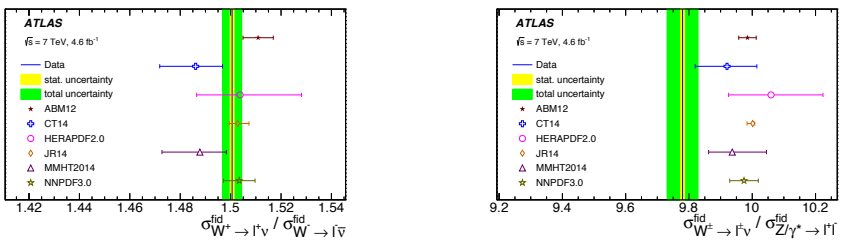

Figure 3: Ratios of the fiducial cross sections times leptonic branching ratios for the W^+ to W^- (left) and for the sum of W^+ and W^- to the Z (right). In both plots, the sum of electron and muon channels is taken. The data (solid blue line) are shown with the statistical (yellow band) and the total uncertainties (green band). Theoretical predictions based on various PDF sets are shown with open symbols of different colours. The uncertainties of the theoretical calculations correspond to the PDF uncertainties only [4].

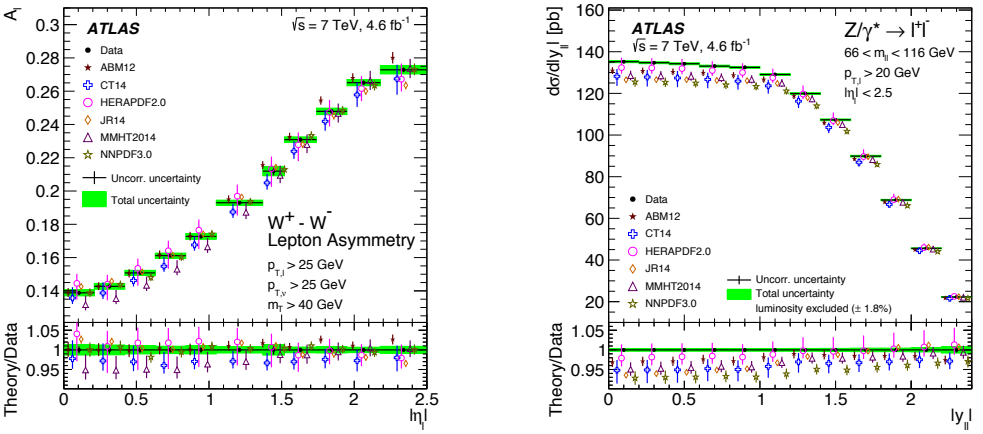

Figure 4: *Left:* Lepton charge asymmetry A_ℓ in $W \to \ell\nu$ production as a function of the lepton pseudorapidity $|\eta_\ell|$. *Right:* Differential cross-section for $Z/\gamma^\star \to \ell^+\ell^-$ production in the Z-peak region, $66 < m_{\ell\ell} < 116$ GeV. Predictions at NNLO QCD with NLO EW corrections using various PDF sets (open symbols) are compared to the data (full points). The ratio of theoretical predictions to the data is also shown. The predictions are displaced within each bin for better visibility. The theory uncertainty is the quadratic sum of the PDF uncertainty and the statistical uncertainty of the calculation [4].

and ℓ^- distributions [4], but has large uncertainties. In the dilepton rapidity distribution of Z decays (see Figure 4, right), almost all predictions are below the observed cross section for $|y| < 1$, and even HERAPDF2.0 is systematically lower, though consistent in each individual rapidity bin due to its' large uncertainty. This can be due to a mismodelling of the fraction of strange quarks in the sea, as suggested by the previous ATLAS observation [13] of an enlarged strangeness fraction in the light quark sea.

The data presented in this analysis are then introduced in the MMHT14 and CT14 PDFs by a procedure called "PDF profiling" (described in Ref. [4]), which provides a shifted set of parton distributions with generally reduced uncertainties. In fact, taking these data into account in these PDFs yields an increased strange fraction $R_s(x) = [s(x) + \bar{s}(x)]/[\bar{u}(x) + \bar{d}(x)]$, towards unity, at the scale $Q^2 = 1.9$ GeV^2; the smallest uncertainty on R_s is obtained for values of Bjorken x around 0.023.

A complete QCD fit analysis is then performed, as described in Ref. [4] and [13], and a brand new PDF set is derived from a combination of the HERA data and the ATLAS data which provide more sensitivity to the flavor composition of the quark sea as well as to the valence-quark distributions at lower x. The new PDF set is termed ATLAS-epWZ16 and at $Q^2 = 1.9$ GeV^2 and $x = 0.023$ it yields $R_s = 1.13 \pm 0.05$ (exp) ± 0.02 (mod) $^{+0.010}_{-0.006}$ (par); experimental (exp) and PDF-fit related uncertainties are reported, where the latter results from the model (mod) and parameterization (par) uncertainties [4]. This result represents an improvement by a factor of three in the experimental uncertainty relative to the previous measurement from the ATLAS-epWZ12 set [13]. Thus, the new PDF set indicates clearly an unsuppressed strangeness at $x = 0.023$, where the current ATLAS W and Z cross section measurements have the largest constraining power. The enhanced strange contribution in the sea leads to a significant reduction of the light quark sea, $x\bar{u} + x\bar{d}$, resulting from the tight

constraint on the sum $4\bar{u} + \bar{d} + \bar{s}$ from the precise measurement of the proton structure function F_2 at HERA.

In addition, this new PDF set allows the determination of the $|V_{cs}|$ parameter, by allowing it to vary freely while all other CKM matrix elements are fixed to the PDG values; it is measured to be $|V_{cs}| = 0.969 \pm 0.013$ (exp) $^{+0.006}_{-0.003}$ (mod) $^{+0.003}_{-0.027}$ (par) $^{+0.011}_{-0.005}$ (thy), where "thy" represents an additional uncertainty due to the extra freedom given to the strange-quark distribution when releasing the assumption that $x\bar{d}(x)$ and $x\bar{s}(x)$ should be the same at low x. In this fit, the R_s value is also determined and it is found consistent with that determined above, when the $|V_{cs}|$ value was fixed assuming CKM unitarity. The precision of this $|V_{cs}|$ measurement is comparable to extractions from charm meson decays (see references in Ref. [4]).

4 Z production in association with jets

The measurement of the production of a Z boson in association with jets, "Z + jets", constitutes a powerful test of perturbative QCD. The large production cross section and easily identifiable decays of the Z boson to charged leptonic final states offer clean experimental signatures which can be precisely measured. Such processes also constitute a non-negligible background for studies of the Higgs boson and in searches for new phenomena; typically in these studies, the multiplicity and kinematics of the jets are exploited to achieve a separation of the signal of interest from the Standard Model Z + jets process, so the latter should be modelled well.

Measurements of Z + jets production cross section in proton-proton collisions at $\sqrt{s} = 13$ TeV are presented here [5], using data corresponding to an integrated luminosity of 3.16 fb^{-1} collected by ATLAS in 2015. Inclusive and differential cross sections are measured for events containing a Z boson decaying to electrons or muons and produced in association with up to seven jets with $p_{\mathrm{T}} > 30$ GeV and $|y| < 2.5$.

Predictions from different Monte Carlo generators based on leading-order (LO) and next-to-leading-order (NLO) matrix elements for up to two additional partons interfaced with parton shower and fixed-order predictions at next-to-leading order and next-to-next-to-leading order (NNLO) are compared with the measured cross sections. In Figure 5 (left) the jet multiplicity is shown, and it is seen that the LO Alpgen+Pythia6 prediction ($Z + \leq 6$ jets) and the NLO predictions by Sherpa 2.2 and MG5_aMC+Pythia8 FxFx do not describe well the high jet multiplicity, where a non-negligible fraction of the jets are from parton shower; instead, the LO generator MG5_aMC+Py8 CKKWL describes the jet multiplicity. The NLO QCD fixed-order calculations from BlackHat+Sherpa predict only up to 4 jets.

On the right side of Figure 5, the leading-jet p_{T} in inclusive $Z+ \geq$ 1,2,3,4 jet events is shown. The "$Z+ \geq 1$ jet Njetti" NNLO perdition and the NLO predictions (BlackHat+Sherpa, Sherpa 2.2,and MG5_aMC+Py8 FxFx) describe well the jet p_{T}, whereas the LO MG5_aMC+Py8 CKKWL generator predicts a too-hard jet p_{T} spectrum at high p_{T}, indicating that the dynamic factorization and renormalization scales, μ_F and μ_R respectively, used in the generation are not appropriate for the full jet p_{T} range.

Other variables which are frequently used to separate either heavier SM particles or beyond-SM physics from the Z + jets process, are also examined in this analysis: angular relations between the two leading jets, dijet massses, as well as quantities based on inclusive p_{T} sums of final-state objects, such as H_{T} (the scalar p_{T} sum of all visible objects in the final state). It is observed that all predictions describe well the mostly back-to-back configuration of the two leading jets, with the recent $Z+ \geq 1$ jet Njetti NNLO prediction describing best all the distributions examined [5].

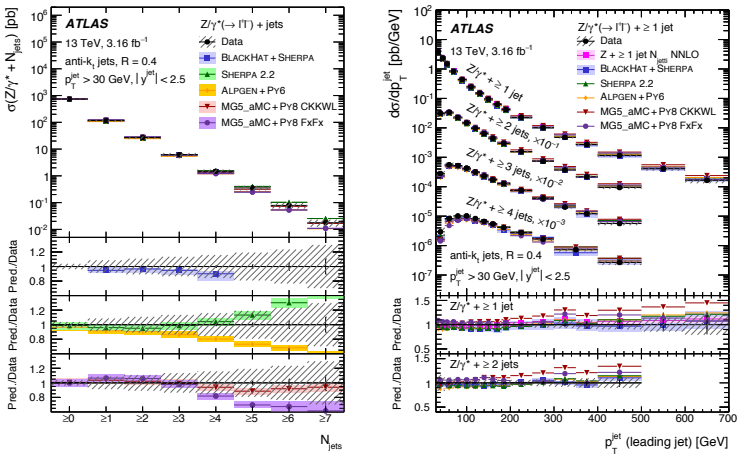

Figure 5. Measured cross section as a function of the inclusive jet multiplicity (left) and as a function of the leading jet p_{T} (right). The data are compared to the predictions described in the text. The error bars correspond to the statistical uncertainty, and the hatched bands to the data statistical and systematic uncertainties (including luminosity) added in quadrature [5].

5 k_{t} splitting scales in Z events

The jet activity in Z events is also studied in ATLAS at different "jet splitting scales"; 20.2 fb^{-1} of pp collisions at 8 TeV are used in this analysis [6].

The k_{t} jet-clustering algorithm starts from a list of particles in the event and at each iteration the number of input objects drops by one (from $k+1$ to k). At each iteration a jet splitting scale d_k is defined as follows [6]. For any two objects i and j in the list, a "distance" d_{ij} is calculated as $d_{ij} = min(p^2_{\mathrm{T},i}, p^2_{\mathrm{T},j}) \times DR^2_{ij}/R^2$, where the minimum of their squared p_{T} values is weighted by the square of the $\eta - \phi$ separation DR_{ij} of the objects relative to a fixed jet-radius R. For each individual object i in the list, the square of its p_{T} is used as its "distance" d_{ib} to the beam axis. Having formed all these distances, at each iteration $k+1 \to k$ the jet splitting scale d_k is the minimum of all the paired- or single- object distances formed; this can be either a two-body distance d_{ij}, in which case the two objects i and j are combined, or it can be the distance of object i to the beam, d_{ib}, in which case the object is removed from the list and it is called a completed jet. The "order" of the jet splitting scale is the iteration step k; e.g., $k = 0$ corresponds to the last iteration step ($1 \to 0$) before the jet-finding algorithm terminates, and so $\sqrt{d_0}$ is the p_{T} of the leading jet in the event. The N^{th} jet splitting scale, d_N, is the distance measure at which an N-jet event can be resolved as an $(N+1)$-jet event.

Differential distributions as a function of the value of the various jet splitting scales are sensitive to the "hard" perturbative modelling (at high values of the splitting scales), as well as to "soft" hadronic activity (at low values of the splitting scales), and they provide complementary input to standard jet measurements. In this measurement [6] such differential cross sections are compared to the theoretical predictions from Sherpa with NLO multijet merging ("MEPS@NLO") and from Powheg+Pythia8 with NNLO matching ("NNLOPS"). On the left side of Figure 6 the differential cross section with respect to $\sqrt{d_0}$ is given; both predictions overshoot significantly the data in the region around 1 GeV, while both of them underestimate the cross section in the peak region (around 3 GeV) by about 10–20%; at 10 GeV they are both consistent with the data, but at higher values the NNLOPS prediction is systematically higher than the data. For higher order splitting scales (see the right side of Figure 6 for $\sqrt{d_7}$), the MEPS@NLO prediction agrees well with the data at the hard region, where the NNLOPS prediction overestimates the cross section. It is also observed that the NNLOPS predictions in the soft region are improved significantly in this high-order splitting scale $\sqrt{d_7}$ compared to the

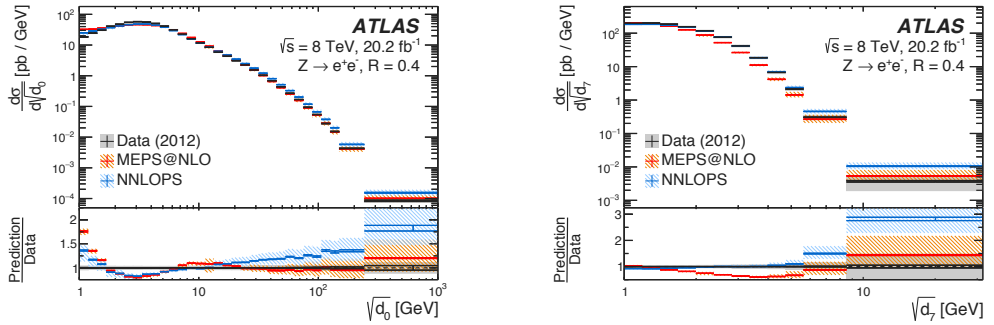

Figure 6: Charged-only distributions for two splitting scales ($\sqrt{d_0}$ on the left, and $\sqrt{d_7}$ on the right) in the electron channel using the jet-radius parameter $R = 0.4$. The size of the error bars reflects the statistical uncertainty, while the combined statistical and systematic uncertainty is indicated by the grey band. Theoretical predictions from Sherpa with NLO multijet merging ("MEPS@NLO") and from Powheg+Pythia 8 with NNLO matching ("NNLOPS") are displayed including error bands for the generator uncertainties [6].

low-order splitting scale $\sqrt{d_0}$. Such comparisons indicate that the data can provide new input for the tuning of the event generators.

6 Triple differential cross section for $Z \to \ell^+\ell^-$ production

This measurement [7] reports the triple-differential cross section for the Drell–Yan process $Z/\gamma^\star \to \ell^+\ell^-$, where ℓ is an electron or a muon. The measurement is performed for invariant masses of the lepton pairs, $m_{\ell\ell}$, between 46 and 200 GeV using a sample of 20.2 fb^{-1} of pp collisions at 8 TeV collected by ATLAS in 2012. The data are presented in bins of the dilepton invariant mass, absolute dilepton rapidity, $|y_{\ell\ell}|$, and the angular variable $\cos\theta^\star$ between the outgoing lepton and the incoming quark in the Collins–Soper frame. The measurements are performed in the range $|y_{\ell\ell}| < 2.4$ in the muon channel, and extended to $|y_{\ell\ell}| < 3.6$ in the electron channel.

Figure 7 shows examples of plots representing the triple differential cross section $d^3\sigma/dm_{\ell\ell}\, d|y_{\ell\ell}|\, d\cos\theta^\star$. Each plot gives the differential cross section as a function of $|y_{\ell\ell}|$, for six bins in $\cos\theta^\star$ and for a specific $m_{\ell\ell}$ range. The combined cross sections are also integrated to produce the single- and double-differential cross sections $d\sigma/dm_{\ell\ell}$ (see Figure 8, left) and $d^2\sigma/dm_{\ell\ell}\, d|y_{\ell\ell}|$. The fiducial cross sections are compared to a theoretical prediction calculated using Powheg at NLO with matched leading-logarithm parton showers. The calculation is approximately corrected for NNLO QCD effects and for additional higher-order electroweak effects using a K-factor which is a function of the dilepton mass. The single- and double-differential measurements are well described by the prediction. Having applied corrections to the scattering amplitude coefficients in Powheg, the prediction also provides a good description of the triple-differential measurements. Specifically in the Z pole region, the measurements achieve a high precision (below the percent level excluding the uncertainty in the integrated luminosity) and are in agreement with predictions.

The triple differential cross section is also used to determine the Z boson forward-backward asymmetry, A_{FB}, as a function of the dilepton mass and rapidity; it is evident from Figure 7 that the cross section difference $\Delta\sigma$ at symmetric $\cos\theta^\star$ bins around $\cos\theta^\star = 0$ flips sign when moving from below to above the Z pole mass. A_{FB} is defined as the difference over the sum of the cross sections between

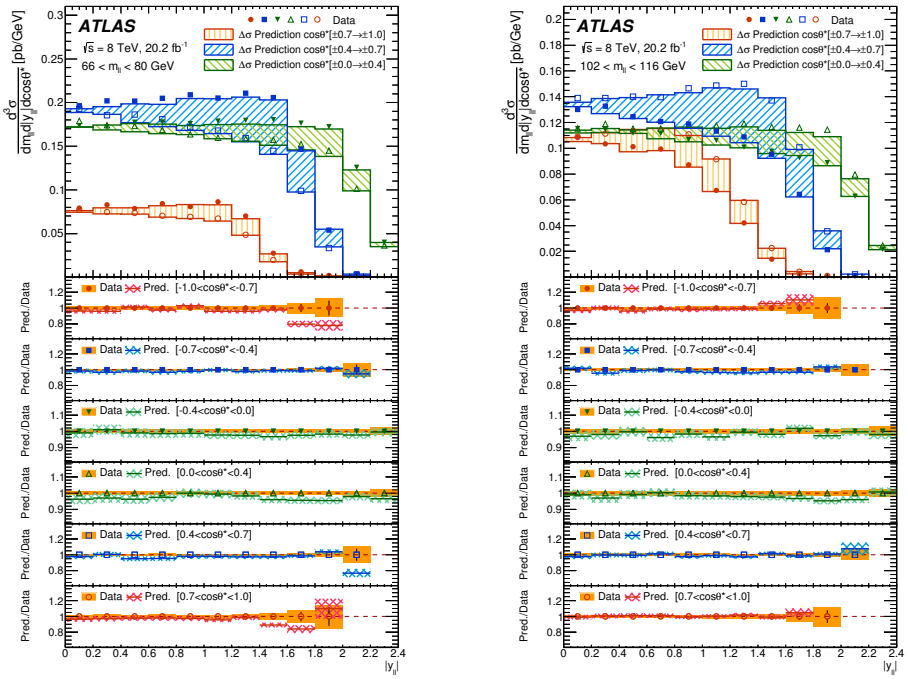

Figure 7: Each plot shows the combined Born-level fiducial cross sections as a function of the dilepton rapidity, $|y_{\ell\ell}|$, for six $\cos\theta^\star$ bins, and for a specific dilepton mass bin; the left plot is below the Z pole, at $66 < m_{\ell\ell} < 80$ GeV, and the right plot is above, at $102 < m_{\ell\ell} < 116$ GeV. The data are shown as solid ($\cos\theta^\star < 0$) and open ($\cos\theta^\star > 0$) markers and the prediction from Powheg including NNLO QCD and NLO EW K-factors is shown as the solid line. The difference, $\Delta\sigma$, between the predicted cross sections in the two measurement bins at equal $|\cos\theta^\star|$ symmetric around $\cos\theta^\star = 0$ is represented by the hatched shading. In each plot, the lower panel shows the ratio of prediction to measurement in each $\cos\theta^\star$ bin. The inner error bars represent the statistical uncertainty of the data and the solid band shows the total experimental uncertainty. The contribution to the uncertainty from the luminosity measurement is excluded. The crosshatched band represents the statistical and PDF uncertainties in the prediction [7].

the full forward ($\cos\theta^\star > 0$) and backward ($\cos\theta^\star < 0$) regions. In Figure 8, right, A_{FB} is shown for $Z/\gamma^\star \to e^+e^-$ events in the forward rapidity region ($1.2 < |y_{\ell\ell}| < 3.6$). The Powheg predictions enhanced with NNLO QCD and NLO EW K-factors describe the observed behaviour of A_{FB} well in all rapidity regions, forming a solid base for a future measurement of the electroweak mixing angle.

7 Conclusions

A collection of recent ATLAS results involving W and Z bosons are presented: a precise measurement of the W mass, matching the single best measurement to-date; inclusive W and Z production measurements; properties of events with jets produced in association with a Z boson; and the triple differential cross section for Z/γ^* Drell-Yan production, as well as the forward-backward asymmetry,

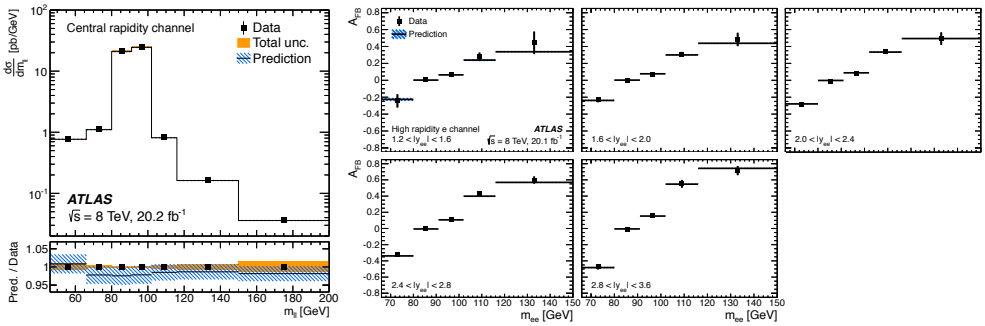

Figure 8: *Left:* Integrated Born-level fiducial cross section $d\sigma/dm_{\ell\ell}$. *Right:* Forward-backward asymmetry, A_{FB}, determined from the combined Born-level fiducial cross section of $Z/\gamma^{\star} \rightarrow e^{+}e^{-}$ production in the forward rapidity region (the kinematic region is labeled in each plot). The data are shown as solid markers and the error bars represent the total experimental uncertainty. The prediction from Powheg including NNLO QCD and NLO EW K-factors is shown as the solid line and the hatched band represents the statistical and PDF uncertainties in the prediction [7].

which forms the base for a future measurement of the electroweak mixing angle. In all cases unprecedented precision is obtained, not only in electroweak parameters, but also in testing perturbative QCD and placing strong constrains in PDFs.

References

[1] ATLAS Collaboration, JINST **3** (2008) S08003.
[2] ATLAS Collaboration, arXiv:1701.07240 [hep-ex], submitted for publication to Eur. Phys. J. **C** (2017).
[3] CDF Collaboration, T. Affolder et al., Phys. Rev. **D 64** (2001) 052001, arXiv:hep-ex/0007044.
[4] ATLAS Collaboration, Eur. Phys. J. **C 77** (2017) 367, arXiv:1612.03016 [hep-ex].
[5] ATLAS Collaboration, Eur. Phys. J. **C 77** (2017) 361, arXiv:1702.05725 [hep-ex].
[6] The ATLAS collaboration, J. High Energ. Phys. **08** (2017) 026, arXiv:1704.01530 [hep-ex].
[7] ATLAS Collaboration, arXiv:1710.05167 [hep-ex], accepted for publication in J. High Energ. Phys. (2017)
[8] Particle Data Group, Chin. Phys. **C, 40**, 100001 (2016).
[9] M. Baak *et al.*, Eur. Phys. J. **C 74** (2014) 3046, arXiv:1407.3792 [hep-ph].
[10] J. de Blas *et al.*, J. High Energ. Phys. **12** (2016) 135. arXiv:1608.01509 [hep-ph].
[11] The ALEPH, DELPHI, L3, OPAL, SLD Collaborations, the LEP Electroweak Working Group, the SLD Electroweak and Heavy Flavour Groups, Phys. Rept. **427** (2006) 257, arXiv:hep-ex/0509008.
[12] CMS Collaboration, Phys. Rev. Lett. **109** (2012) 111806, arXiv:1206.2598 [hep-ex], and Phys. Rev. D **90** (2014) 032004, arXiv:1312.6283 [hep-ex].
[13] ATLAS Collaboration, Phys. Rev. Lett. **109** (2012) 012001, arXiv:1203.4051 [hep-ex].